Published in final edited form as:
Ultrasound Med Biol. 2011 March ; 37(3): 393–402. doi:10.1016/j.ultrasmedbio.2010.11.011.

GENE THERAPY OF CARCINOMA USING ULTRASOUND-TARGETED MICROBUBBLE DESTRUCTION

Andrew R. Carson[*], **Charles F. McTiernan**[*], **Linda Lavery**[*], **Abigail Hodnick**[*], **Michelle Grata**[*], **Xiaoping Leng**[*], **Jianjun Wang**[*], **Xucai Chen**[*], **Ruth A. Modzelewski**[†], and **Flordeliza S. Villanueva**[*]

[*]Center for Ultrasound Molecular Imaging and Therapeutics, Cardiovascular Institute, University of Pittsburgh Medical Center

[†]Pittsburgh Cancer Institute University of Pittsburgh, Pittsburgh, PA

Abstract

When microbubble contrast agents are loaded with genes and systemically injected, ultrasound-targeted microbubble destruction (UTMD) facilitates focused delivery of genes to target tissues. A mouse model of squamous cell carcinoma was used to test the hypothesis that UTMD would specifically transduce tumor tissue and slow tumor growth when treated with herpes simplex virus thymidine kinase (TK) and ganciclovir. UTMD-mediated delivery of reporter genes resulted in tumor expression of luciferase and green fluorescent protein (GFP) in perivascular areas and individual tumor cells that exceeded expression in control tumors ($p = 0.02$). The doubling time of TK-treated tumors was longer than GFP-treated tumors ($p = 0.02$), and TK-treated tumors displayed increased apoptosis ($p = 0.04$) and more areas of cellular drop-out ($p = 0.03$). These data indicate that UTMD gene therapy can transduce solid tumors and mediate a therapeutic effect. UTMD is a promising nonviral method for targeting gene therapy that may be useful in a spectrum of tumors.

Keywords

Nonviral vectors; Ultrasound contrast agents; Ultrasound imaging; Targeting strategies; Squamous cell carcinoma; Suicide genes

INTRODUCTION

Gene therapy is a promising approach for destroying tumor cells in a variety of cancers but requires improvements in delivery techniques to enable clinical application (Thomas and Grandis 2009). The suicide gene, herpes simplex virus–1 thymidine kinase (TK), in conjunction with ganciclovir (GCV), has been studied for gene therapy of cancer in several clinical trials (Rainov 2000; Shand et al. 1999). Despite their promise, these studies are

Address correspondence to: Flordeliza S. Villanueva, M.D., University of Pittsburgh, Cardiovascular Institute, University of Pittsburgh Medical Center, Center for Ultrasound Molecular Imaging and Therapeutics, A351 Presbyterian University Hospital, 200 Lothrop Street, Pittsburgh, PA 15213. villanuevafs@upmc.edu.

disadvantaged by the requirement for surgical access to inject gene vectors directly into the tumor, which is not always technically feasible and limits the possibility of multiple treatments. Alternatively, if viral gene therapy vectors are delivered systemically, transduction of nontarget tissues may occur, resulting in adverse side effects (Parryl et al. 2009). Viral vectors also elicit an immune response that can limit their effectiveness and prevent repeated delivery (Nayak and Herzog 2010). An ideal gene therapeutic approach would be nonviral based and capable of specifically targeting and destroying tumor cells after systemic delivery, while leaving nontarget organs unaffected.

Ultrasound contrast agents, gas-filled microspheres (microbubbles) encapsulated by a biocompatible shell, are emerging as new gene therapy vectors that may overcome some of the limitations of viral gene delivery systems (Chen et al. 2010; Villanueva 2009). Microbubbles are used in echocardiographic imaging as erythrocyte “tracers” that transit through the circulation (Jayaweera et al. 1994; Kaul 2008). The contrast enhancement created by the microbubbles during clinical ultrasound imaging is based on their acoustic activity whereby the microbubbles expand and contract, or rupture, in response to ultrasound (Becker and Burns 2000; de Jong et al. 2002). More recently, this acoustic behavior of ultrasound contrast agents has been exploited for therapeutic purposes, and a number of studies have shown that microbubbles carrying genes on their surface facilitate transduction when ultrasound is externally applied as the microbubbles transit through the target site microcirculation (Bekeredjian et al. 2003; Chappell and Price 2006; Chen et al. 2007, 2010; Fujii et al. 2009).

The use of microbubbles as gene vectors is based on the hypothesis that destruction of DNA-loaded microbubbles by a focused ultrasound beam during their microvascular transit through the target area will result in localized transduction upon disruption of the microbubble shell while sparing non-targeted areas. Ultrasound-targeted microbubble destruction (UTMD) has been used to deliver genes to cells *in vitro* and more recently has been used to deliver genes *in vivo* to treat diabetes and cardiovascular disease in experimental animal models (Chen et al. 2006; Chen et al. 2010; Fujii et al. 2009). Because this noninvasive, site-specific, nonviral approach to gene delivery could have significant value for treating tumors, we tested the general hypothesis that UTMD-mediated gene delivery can be used to treat solid tumors. Specifically, we investigated whether UTMD-mediated delivery of the suicide gene TK to tumors, in conjunction with GCV treatment, retards tumor growth in a mouse model of squamous cell carcinoma. Reporter gene studies were first performed to confirm transduction and develop the ultrasound treatment protocol. These were followed by proof of concept studies in which the TK gene was delivered *via* UTMD and the effect on tumor growth was assessed.

MATERIALS AND METHODS

Microbubble preparation and confirmation of DNA binding

DNA binding microbubbles were prepared from a mixture of 1,2-distearoyl-sn-glycero-3-ethylphosphocholine (Avanti Lipids, Alabaster, AL, USA), distearoylphosphatidyl-choline (Avanti Lipids) and poly-ethylene glycol-40 (Sigma, St. Louis, MO, USA) in phosphate-buffered saline (PBS) containing 1 mM ethyl-enediamine tetraacetic acid (EDTA). This

solution was placed in a glass vial, the head space was replaced with perfluorobutane gas and the mixture was amalgamated to form perfluorobutane lipid-encapsulated microbubbles. Microbubbles were then centrifuged, washed three times with PBS/EDTA and resuspended in PBS/EDTA, resulting in a microbubble concentration of $1–4 \times 10^9$/mL and diameter of 1.9–2.3 μm as measured by Coulter counting (Beckman Coulter, Brea, CA, USA). Plasmid DNA was attached by mixing plasmid (100 μg) and 1×10^9 microbubbles and briefly vortexing. The following plasmid constructs were used: pEGFP-C1 (Clontech, Mountain View, CA, USA), which contains the green fluorescent protein (GFP) gene driven by the CMV promoter; pCMV-Luc, in which the GFP gene in pEGFP-C1 was replaced with a firefly luciferase gene; and pCMV-TK, in which the GFP gene in pEGFP-C1 was replaced with the herpes simplex virus–1 TK gene. DNA binding to the microbubbles was confirmed by serial washing at different time points up to eight hours after DNA attachment and recovering DNA from both bound and unbound (wash) fractions using chloroform/isoamyl alcohol (24:1) fractionation to burst microbubbles and remove lipid components. Equivalent sample volumes were then analyzed for DNA content by standard agarose gel electrophoresis followed by ethidium bromide staining.

DNAse I protection assay

To determine whether plasmid DNA on the surface of a microbubble might be protected from DNases present in the circulation, DNA-loaded microbubbles were prepared as described above, with 50 μg DNA resuspended in l mL reaction buffer containing 10 mM Tris 7.6 and 2.5 mM $MgCl_2$ and challenged with a range of DNase I concentrations from 0.0003–1 U/mL (New England Biolabs, Ipswich, MA, USA). As a positive control, 50 μg DNA was challenged under the same conditions in the absence of microbubbles.

Luciferase assays

Luciferase expression was quantified using the Promega Luciferase Assay System (Promega, Madison, WI, USA). Briefly, tissue samples were homogenized, protein content was estimated by Bradford assay and luciferase activity was detected using a luminometer with a 20-s sampling time. Raw luciferase activity (RLU) was subtracted from background readings obtained from resuspension buffer alone and expressed as RLU/min/mg of protein.

Histologic analyses

Immunofluorescent and histochemical staining—Immunofluorescent staining was used to confirm transduction of GFP and identification of vascular or lymphatic endothelial cells. Tumor samples were frozen in optimal cutting temperature media, sectioned, fixed with 10% formalin, blocked, washed and incubated with primary antibody for GFP (Invitrogen, Carlsbad, CA, USA); the endothelial markers von Willebrand factor (vWF) (Dako, Carpinteria, CA, USA) or biotinylated Griffonia Simplicifolia Lectin I (Vector Labs, Burlingame, CA, USA); the macrophage marker CD68 (Abcam, Cambridge, MA, USA); or the lymphatic marker LYVE1 (Abcam). After washing, slides were incubated with either secondary anti-rabbit FITC conjugate (Molecular Probes, Eugene, OR, USA) or Strepavidin-FITC conjugate (Sigma), washed, counterstained with DAPI, had coverslips added and were visualized on an Olympus IX81 microscope (Center Valley, PA, USA) interfaced with

digital CCD camera (Olympus DP71). TUNEL analysis was performed using the ApopTag kit according to vendor protocols (Millipore, Billerica, MA, USA) to identify apoptotic cells (Gavrieli et al. 1992).

Structural characterization of tumors—Standard hematoxylin and eosin (H&E) staining was performed on 6-μm tumor sections. During initial H&E staining, treated tumors were noted to have scattered areas of cell dropout. To standardize definitions and further quantify this phenomenon, we defined these acellular areas as having maximum diameters greater than 25 μm and a short-axis-to-long-axis ratio of <1:4, to distinguish them from small cracks caused by tissue processing. The acellular zones defined as such were counted, the total area of each cross section was determined and the number of acellular zones was calculated as zones per mm^2. Formalin-fixed sections were stained with 0.2% Oil Red O (Sigma) or Gomori Trichrome (Protocol, Kalamazoo, MI, USA) to detect adipose cells or fibrosis, respectively, in the cell drop-out areas (Gomori 1950). To determine whether areas of cell drop-out were connected to the systemic circulation, the intravascular stain Hoescht 33342 (8 μg/g) was injected intravenously 6 min before euthanasia and tissue harvest (Reinhold and Visser 1983).

Mouse tumor model

The animal protocols were approved by the University of Pittsburgh Institutional Animal Care and Use Committee and conformed to the PHS Policy on the Humane Care and Use of Laboratory Animals. Mouse squamous cell tumors were induced as previously described (Fu et al. 1984). Mouse squamous cell carcinoma cells were cultured and passed no more than four times *in vitro* before use. C3H/NeJ mice received subcutaneous injection of 5×10^5 carcinoma cells over the dorsal surface of the thoracic/lumbar spine under isofluorane anesthesia. In this model, tumors typically grow to 0.5 mL by 10–12 d after injection. On the day of gene therapy, animals were re-anesthetized, and the jugular vein was cannulated. After injection, mice were recovered and administered 0.6 mg/kg intraperitoneal buprenorphine daily for 3 d post surgery.

Serial measurement of tumor volume

The mice were anesthetized with isofluorane and positioned for imaging. Cross-sectional ultrasound images (14 MHz; Sequoia, Siemens Corp, Mountain View, CA, USA) of the tumor were digitally acquired by fixing the transducer to a microstage manipulator with millimeter calibrations and moving the transducer at 1-mm increments along the long axis of the tumor. Areas from each 1-mm-thick cross section were planimetered and summed to yield the total tumor volume. This approach was chosen over conventional caliper measurements because they do not assume an elliptical tumor shape and the imaging can visualize full tumor thickness below the skin.

Ultrasound transduction treatment protocol

Daily measurement of tumor volume was initiated 7 d after injection of the tumor cells and UTMD commenced when tumor volume was 0.1–0.15 mL by ultrasound measurement. Microbubbles (1 mL) were infused into the jugular vein over 20 min in conjunction with ultrasound delivery to the tumor over 30 min. Ultrasound imaging was combined with

UTMD using a two-transducer system to perform concurrent high-frequency, low-power 2-D perfusion imaging and lower-frequency, high-power microbubble destruction. Specifically, microbubble perfusion of the tumor was visualized in real time using ultrasound (7 MHz; Contrast Pulse Sequencing, Sequoia, Siemens Corp) at a low acoustic power (mechanical index 0.4) to minimize microbubble destruction. Upon visualization of microbubbles within the tumor, microbubbles were burst using an orthogonally placed ultrasound transducer (S3 probe, Sonos 7500, Philips, Andover, MA, USA) delivering ultrasound at 1.3 MHz and a mechanical index (MI) of 1.6, with the 7-MHz imaging transducer confirming successful microbubble destruction. Destructive ultrasound bursts were repeated each time microbubble replenishment of the tumor was visualized. The interval between destructive ultrasound bursts was adjusted to allow full microbubble reperfusion of the tumor before the next burst cycle. The number of destructive ultrasound bursts was adjusted to the minimum number required to destroy most bubbles in the tumor as visualized during concurrent low MI imaging. Thereafter, the venous cannula was removed and the mice were recovered.

Experimental groups

Nine mice were first used to determine the extent and location of UTMD-mediated transduction using microbubbles loaded with pCMV-Luc (luciferase, $n = 6$) and pEGFP-C1 (GFP, $n = 3$), respectively. Eight control mice received the identical microbubble injection (luciferase, $n = 5$ and GFP, $n = 3$), but no ultrasound. Mice were euthanized 3 d later and the tumors were harvested. Therapeutic studies were performed in mice ($n = 5$) that were administered intravenous microbubbles loaded with pCMV-TK and treated with UTMD. Control mice received UTMD ($n = 6$) using microbubbles loaded with pEGFP-C1. Both groups were administered GCV (80 mg/kg) intraperitoneally daily for the duration of the protocol, commencing 3 d after UTMD. Tumor volume was serially measured and mice were euthanized and the tumor was harvested when tumor volume reached 2 mL. A separate group of four mice ($n = 2$ TK, $n = 2$ GFP) were euthanized 3 d after microbubble delivery and UTMD treatment, but before GCV treatment, to evaluate tumor morphology early after UTMD.

Statistical methods

Data are expressed as mean ± standard deviation. Means were compared using two-tailed Student's *t*-test (unpaired), with significance defined as $p < 0.05$. To calculate tumor doubling time for individual tumors, tumor volume measurements (y) were plotted as a function of time (t) and fit to the exponential function $y = X_0 \cdot e^{kt}$, where X_0 is the tumor volume at time 0. Doubling time (Dt) was calculated as Dt =ln2/k. Group sizes were determined by *a priori* power analysis using doubling times (~3 d) and standard deviations (~10%) from preliminary studies. Using these estimates, group sizes of at least five are appropriate to detect a 20% or more difference in tumor doubling time with a power of ~90%.

RESULTS

Efficiency of DNA-microbubble binding

The microbubble formulation bound ~100 μg DNA per 1×10^9 microbubbles. Attempts to bind larger amounts of DNA resulted in similar levels of DNA loading, indicating that microbubbles approach saturation at this concentration. By gel electrophoresis, there was minimal DNA in the washes performed shortly after the attachment procedure, with no plasmid release over a four-hour period and minimal release up to eight hours later (Fig. 1). Plasmid DNA attached to microbubbles was protected from DNAse I digestion at concentrations much greater than that required for the complete digestion of uncomplexed plasmid DNA (Fig. 2).

Reporter gene expression

Tumor luciferase activity was significantly greater in the six mice receiving microbubbles bearing pCMV-Luc plus UTMD (1568 ± 627 RLU/min/mg) compared with the five control mice receiving microbubbles with pCMV-Luc but no ultrasound (294 ± 807 RLU/min/mg, $p = 0.02$). Tumor luciferase activity in the mice receiving pCMV-Luc–loaded microbubbles and ultrasound was also significantly higher than activity in noninsonified, nontumor tissue obtained from these same mice ($p < 0.02$) (Fig. 3). GFP was identified in cells located in and around areas comprising the walls of structures resembling vasculature ranging in diameter from 25 μm to >100 μm (Fig. 4a), as well as in tumor cells (Fig. 4b). Tumors from the control group not receiving UTMD displayed no GFP staining (Fig. 4c). Likewise, noninsonified, nontumor tissue obtained from mice injected with GFP plasmid–loaded microbubbles and treated with tumor-directed UTMD displayed no GFP staining (data not shown).

Tumor response to TK transduction and GCV treatment

Figure 5 illustrates tumor growth after transduction of the GCV-treated mice receiving UTMD-gene delivery of pCMV-TK (TK/GCV group) or pEGFP-C1 (GFP/GCV group) from an initial size of 0.1–0.15 mL (Day 0) until the mice were euthanized. Tumor growth rates were similar in both TK- and GFP-treated mice from days 0–3, and began to diverge at day 3, when GCV treatment was initiated. From days 3–10, the doubling time of the TK/GCV-treated tumors (3.4 ± 0.2 d) was significantly greater than that of control GFP/GCV-treated tumors (2.9 ± 0.4 d; $p < 0.02$).

Histological evaluation

H&E stains revealed scattered regions of cell dropout in the TK-treated tumors (Fig. 6a). When these acellular areas were categorized based on dimensions as described above, there were significantly more such zones in the TK/GCV group than in the GFP/GCV controls (Fig. 6b) ($3.8 \pm 2.1/mm^2$ *vs.* $1.3 \pm 1.0/mm^2$, $p < 0.03$). This three-fold difference in the density of acellular zones occurred despite a comparable initial density of acellular zones in the four mice that were euthanized on day 3 after UTMD treatment (TK = 0.2 zones/mm^2, GFP = 0.2 zones/mm^2). The acellular zones stained negatively for fat (Oil Red O), fibrosis (Gomori Trichrome), macrophages (CD68) and lymphatic markers (LYVE-1). Most (~90%)

of the acellular zones also stained negatively for the endothelium marker vWF (Fig. 6d) or the endothelium binding lectin Griffonia Simplicifolia Lectin I (GSLI) (data not shown). Hoescht 33342 stain injected intravenously ante-mortem appeared in the periphery of these acellular zones, indicating continuity with the systemic vascular circulation (Fig. 6c), despite the fact that many such zones stained negatively for endothelium. Many of the acellular areas were similar in morphology to areas that were GFP-positive in the reporter gene transduction studies described previously (Fig. 4a). TUNEL assay indicated that TK/GCV-treated mice (Fig. 7a) had more apoptotic nuclei than control GFP/GCV-treated mice (Fig. 7b) (6 ± 1 *vs.* $4 \pm 1\%$ apoptotic nuclei; $p = 0.04$).

DISCUSSION

The main finding of this study is that UTMD can direct delivery of the suicide gene TK to tumor cells, ultimately decelerating tumor growth in a murine model of squamous cell carcinoma. These findings establish proof of concept that UTMD can impact tumor biology. As such, our study has promising implications for gene therapy–based treatments for cancer, supporting a potential role for microbubble carriers as nonviral vectors with inherent targeting properties by virtue of their unique acoustic behavior in an ultrasound field.

The use of microbubbles as gene vectors has advantages over viral systems. During UTMD, intravenously injected microbubbles are destroyed as they transit through the microcirculation of the target site where the ultrasound beam is directed, functionally achieving selective payload delivery without the need for invasive approaches such as direct intratumor injection. The lipid microbubbles we used for UTMD have no viral proteins, and can theoretically be administered repetitively. In addition, because the microbubbles are ultrasound contrast agents, it is possible to simultaneously image microbubble transit through the tumor, thereby enabling more precise real-time guidance of plasmid delivery.

The mechanisms underlying UTMD-mediated gene transfer are incompletely understood. Although it is clear that ultrasound-induced destruction of the plasmid-bearing microbubbles is a necessary event, it not certain how or if the genes transgress the endothelial barrier after microbubble destruction. Christiansen et al. (2003) reported intravital imaging of rat cremaster microcirculation during UTMD of microbubbles bearing fluorescently labeled DNA, in which DNA deposition was observed to be perivascular in location with only 10–15% of the depositions associated with microvascular hemorrhage. Independent of gene release, UTMD can induce changes in the membranes of treated cells, leading to sporadic capillary ruptures and/or increased permeability to macromolecules (Meijering et al. 2009; Price et al. 1998; van Wamel et al. 2004). Microbubble disruption at ultrasound frequencies used in our study can produce high local pressure currents (jetting) or high-velocity fragmentation of the microbubble shell, which may also contribute to the transduction event (Zhao et al. 2005). Taken together, such data suggest that microporation of the vessel wall and/or enhanced permeability of cell membranes may be a mechanism for transfection by UTMD. Although Christiansen et al. (2003) observed a small portion of DNA deposition to anatomically colocalize with microvascular hemorrhage with UTMD, and others have posited ultrasound-microbubble–induced microvascular hemorrhage as a mechanism for drug or particle delivery (Price et al. 1998) using very different ultrasound and *in vivo*

testing conditions compared with ours, we did not observe microvascular hemorrhage in our study.

We sought to custom design microbubbles capable of delivering large amounts of DNA by incorporating positively charged lipids into the microbubble shell. The resulting microbubble formulation efficiently bound nearly 100 μg DNA per 1×10^9 microbubbles, which is significantly higher compared with reports of others (Hayashi et al. 2009; Maeda et al. 2009). Importantly, unlike naked plasmids, which are quickly degraded by blood DNAses upon vascular administration, our data showed that the plasmid on the microbubble surface was shielded from digestion by DNAse. The DNAse protection would indicate a close and tight binding of the DNA to the microbubble, which is supported by ethidium bromide staining studies (data not shown), demonstrating DNA association with microbubble shell. It is expected that the negatively charged plasmid DNA would preferentially associate with the cationic lipid heads in these microbubbles. Although it is possible that there might be some burial of the plasmid under the lipid heads, it is unlikely that the hydrophilic DNA would preferentially reside in close proximity with the hydrophobic core of a microbubble. Furthermore, because we add the plasmid DNA to the formulation *after* the microbubbles have already been synthesized, it is unlikely that plasmid DNA would be “trapped” in the gas-filled interior of a microbubble.

Before performing therapeutic studies, we delivered the luciferase gene to tumors to quantify transgene expression. Using the ultrasound exposure conditions described in this report to transduce tumors, we achieved a level of luciferase expression that is consistent with other reports of UTMD gene delivery to other organ systems when microbubbles are delivered systemically (Bekeredjian et al. 2003). Our data demonstrated that specific targeting is achieved by navigation of the ultrasound beam, because there was minimal reporter gene transduction in noninsonified tissues. Furthermore, the control group receiving only DNA-loaded microbubbles had very little tumor expression of luciferase, underscoring the importance of the ultrasound in transduction.

We identified GFP transduction both in tumor cells and cells bordering acellular areas displaying a vascular morphology, many of which correspond to the acellular zones that were abundant in the TK/GCV-treated group (Fig. 4a, Fig. 6a). Although the staining of these zones for the vascular markers vWF and Griffonia Simplicifolia Lectin I was variable, approximately 90% of these structures stained positive upon *in vivo* injection of Heoscht dye, indicating anatomic continuity with the systemic circulation (Fig. 6c). A pattern of positive staining for perfusion with negative staining for endothelium is not unusual for tumor vasculature and it is likely that many of these structures were conduits for blood and microbubbles at the time of transduction (Bhattacharya et al. 2008). The GFP data thus indicate both vascular as well as direct cellular transduction, which is consistent with the intra-vital microscopic observations of DNA deposition reported by Christiansen et al. (2003).

We then sought to determine whether plasmid-loaded microbubbles and our ultrasound protocol could effect a therapeutic change in tumor growth in a murine squamous cell carcinoma model. Upon UTMD-mediated delivery of the suicide gene herpes simplex virus

TK, and treatment with GCV, there was a small but significant increase in the doubling time of TK/GCV-treated tumors compared with GFP/GCV controls. We sought to further understand the mechanism of tumor growth reduction through additional histological analysis. TK/GCV-treated tumors demonstrated an increase in the number of acellular areas upon GCV treatment. These zones of clearing could represent damaged remnants of vasculature destroyed by TK/GCV treatment. Some of these zones could also represent drop-out of TK/GCV-treated tumor cells that have been subsequently cleared. This drop-out would be further augmented by the bystander effect, which may enlarge these zones through the leakage of phosphorylated GCV through gap junctions into neighboring tumor cells (Rainov 2000; Aoi et al. 2008). Given that the Hoescht stains demonstrated access of these zones to the systemic circulation, there is a strong possibility that killed cells were cleared into the circulation. Because control tumors also demonstrated acellular zones, albeit significantly fewer (Fig. 6), it is unlikely that all of these areas represented treatment-specific cellular dropout; some may represent tumor vasculature. TUNEL staining revealed a modest (1.5-fold) but statistically significant increase in apoptosis throughout TK/GCV-treated tumors compared with controls, which could also contribute to the overall growth inhibition.

To our knowledge, this is the first report using intravenous injection of plasmid-loaded microbubbles and ultrasound to treat malignant tumors. Some studies have used UTMD-mediated gene therapy to solid tumors *via* a direct intratumor injection followed by ultrasound delivery (Chen et al. 2009a, 2009b; Li et al. 2009). This invasive approach, however, does not take advantage of the noninvasive nature of systemic microbubble injection combined with local ultrasound to achieve targeted delivery. Another group has used adenovirus virus–loaded microbubbles and ultrasound to treat tumors (Greco et al. 2010), but the use of viral vectors may be immunogenic and less attractive than a purely nonviral delivery system.

Several limitations to this study should be mentioned. The amount of transduction detected using reporter genes was relatively limited, and the level of tumor growth inhibition was correspondingly modest. Nonetheless, the extent of reporter gene expression in our study was similar to that published by others using UTMD (Bekeredjian et al. 2003). It should be emphasized that our data prove the concept that UTMD can alter the natural history of tumor growth. Also, some of the therapeutic benefit in our system could be a result of the “bystander effect,” which may partially compensate for low transduction efficiency and partly explain the growth retardation we observed despite the limited transduction levels. Importantly, it is likely that additional optimization of UTMD parameters, such as inclusion of targeting ligands (Villanueva and Wagner 2008; Weller et al. 2002, 2005), enhancement of ultrasound conditions or modification of the treatment schedule may enhance plasmid delivery and improve transduction efficiency. These steps, although important, are beyond the scope of this study and will require further research. Although the magnitude of growth delay upon TK/GCV treatment of this innately fast-growing tumor line was less than what has been reported for viral vectors in other tumor lines (Rainov 2000), it is similar to the growth delay induced by established tumor treatments, such as paclitaxel, in this tumor model (Hershberger et al. 2001).

The decrease in tumor growth in the current study was also less than has been reported for the alternate invasive approach using direct intratumor injection of microbubbles (Aoi et al. 2008; Nie et al. 2008). Reduced transduction compared with the direct injection technique might be caused by reduced plasmid and microbubble concentration in the tumor, because the delivery of plasmid-loaded microbubbles is dependent on tumor perfusion. Also, because the tumor must be allowed to reperfuse with microbubbles before each destructive ultrasound sequence is initiated, the total ultrasound energy delivered is less than that achieved with direct injection techniques. Lastly, as microbubbles are delivered though the bloodstream in our system, vascular endothelium (if present) may act as a barrier to plasmid delivery. Nevertheless, the advantage of our approach is that it does not use viral vectors, and it does not require direct tumor injection, which has practical value for tumors that are difficult to access and/or may require serial treatments.

With further optimization of treatment parameters along the lines mentioned here, therapeutic results are likely to be enhanced beyond our proof of concept study. It is likely that greater numbers of microbubbles could be delivered to the tumor by direct arterial cannulation of the tumor blood supply. Although direct cannulation is more invasive, it is possible that greater levels of transduction might make this approach attractive for tumors with easily identifiable and accessible arterial blood supplies. Furthermore, it is likely that TK/GCV is not the most potent gene in this system and the attachment and delivery of optimal anticancer genes should be considered. It should be noted that few anticancer drugs or treatments are very effective alone, and the small decrease in growth seen when our system is used in isolation could lead to greater growth inhibition when used adjuvantly with other treatments.

Finally, another limitation is that histological evaluation of tumors at the time of euthanasia only sheds partial light on the mechanisms of growth inhibition that would have begun days earlier. We cannot, therefore, rule out the possibility that apoptosis predominated earlier in the course of the tumors, when transgene expression would be highest. Taken as a whole, antivascular effects, direct TK/GCV mediated cell killing and any bystander effects are not mutually exclusive, and all of these mechanisms may have contributed to the observed tumor growth inhibition.

In conclusion, gene therapy using microbubbles as vectors and ultrasound to direct local transfer of the genes to the target site is a promising strategy that could circumvent limitations of viral gene delivery systems. By injecting microbubbles systemically, the technique is minimally invasive and is, in theory, easily adapted to serial treatments. The ability to focus treatment by manipulating the direction of the ultrasound beam is particularly attractive for nonresectable, inaccessible tumors in which direct intratumor or intra-arterial injection of therapeutics is not technically feasible. Our data establish important proof of the principle that it is possible to modify the natural history of tumor growth with UTMD-directed gene therapy, and also provide insights into factors that may be important to the optimization of transduction under conditions of systemic microbubble injection.

Acknowledgments

This study was supported in part by a postdoctoral fellowship grant from the American Heart Association, Great Rivers Affiliate (Dr. Carson) and by the Center for Ultrasound Molecular Imaging and Therapeutics, University of Pittsburgh Medical Center and University of Pittsburgh. Dr. Villanueva is supported in part by the National Institutes of Health (RO1HL077534-01).

References

Aoi A, Watanabe Y, Mori S, Takahashi M, Vassaux G, Kodama T. Herpes simplex virus thymidine kinase-mediated suicide gene therapy using nano/microbubbles and ultrasound. Ultrasound Med Biol. 2008; 34:425–434. [PubMed: 18096302]

Becker, H.; Burns, PN. Handbook of contrast echocardiography. New York: Springer-Verlag; 2000.

Bekeredjian R, Chen S, Frenkel PA, Grayburn PA, Shohet RV. Ultrasound-targeted microbubble destruction can repeatedly direct highly specific plasmid expression to the heart. Circulation. 2003; 108:1022–1026. [PubMed: 12912823]

Bhattacharya A, Seshadri M, Oven SD, Tóth K, Vaughan MM, Rustum YM. Tumor vascular maturation and improved drug delivery induced by methylselenocysteine leads to therapeutic synergy with anticancer drugs. Clin Cancer Res. 2008; 14:3926–3932. [PubMed: 18559614]

Chappell JC, Price RJ. Therapeutic applications of acoustically active microspheres in the microcirculation. Microcirculation. 2006; 13:57–70. [PubMed: 16393947]

Chen S, Ding JH, Bekeredjian R, Yang BZ, Shohet RV, Johnston SA, Hohmeier HE, Newgard CB, Grayburn PA. Efficient gene delivery to pancreatic islets with ultrasonic microbubble destruction technology. PNAS. 2006; 103:8469–8474. [PubMed: 16709667]

Chen S, Ding JH, Yu C, Yang B, Wood DR, Grayburn PA. Reversal of streptozotocin-induced diabetes in rats by gene therapy with betacellulin and pancreatic duodenal homeobox-1. Gene Ther. 2007; 14:1102–1110. [PubMed: 17460716]

Chen S, Shimoda M, Wang M, Ding J, Noguchi H, Matsumoto S, Grayburn PA. Regeneration of pancreatic islets in vivo by ultrasound-targeted gene therapy. Gene Ther. 2010; 17:1411–1420. [PubMed: 20508600]

Chen Z, Liang K, Liu J, Xie M, Wang X, Lü Q, Zhang J, Fang L. Enhancement of survivin gene downregulation and cell apoptosis by a novel combination: Liposome microbubbles and ultrasound exposure. Med Oncol. 2009a; 26:491–500. [PubMed: 19137432]

Chen ZY, Liang K, Xie MX, Wang XF, Lü Q, Zhang J. Induced apoptosis with ultrasound-mediated microbubble destruction and shRNA targeting survivin in transplanted tumors. Adv Ther. 2009b; 26:99–106. [PubMed: 19083158]

Christiansen JP, French BA, Klibanov AL, Kaul S, Lindner JR. Targeted tissue transfection with ultrasound destruction of plasmid-bearing cationic microbubbles. Ultrasound Med Biol. 2003; 29:1759–1767. [PubMed: 14698343]

de Jong N, Ayache Bouakaz, Frinking P. Basic acoustic properties of microbubbles. Echocardiography. 2002; 19:229–240. [PubMed: 12022933]

Fu KK, Rayner PA, Lam KN. Modification of the effects of continuous low dose rate irradiation by concurrent chemotherapy infusion. Int J Radiat Oncol Biol Phys. 1984; 10:1473–1478. [PubMed: 6206039]

Fujii H, Sun Z, Li SH, Wu J, Fazel S, Weisel RD, Rakowski H, Lindner J, Li RK. Ultrasound-targeted gene delivery induces angiogenesis after a myocardial infarction in mice. J Am Coll Cardiol Cardiovasc Imaging. 2009; 2:869–879.

Gavrieli Y, Sherman Y, Ben-Sasson SA. Identification of programmed cell death in situ via specific labeling of nuclear DNA fragmentation. J Cell Biol. 1992; 119:493–501. [PubMed: 1400587]

Gomori G. A rapid one-step trichrome stain. Am J Clin Pathol. 1950; 20:661–663. [PubMed: 15432364]

Greco A, Di Benedetto A, Howard CM, Kelly S, Dementieva Y, Miranda M, Brunetti A, Salvatore M, Claudio L, Sarkar D, Fisher PB, Claudio PP. Eradication of therapy-resistant human prostate

tumors using an ultrasound-guided site-specific cancer terminator virus delivery approach. Mol Ther. 2010; 18:295–306. [PubMed: 19888195]

Hayashi S, Mizuno M, Yoshida J, Nakao A. Effect of sonoporation on cationic liposome-mediated IFNbeta gene therapy for metastatic hepatic tumors of murine colon cancer. Cancer Gene Ther. 2009; 16:638–643. [PubMed: 19498458]

Hershberger PA, Yu WD, Modzelewski RA, Rueger RM, Johnson CS, Trump DL. Calcitriol (1,25-dihydroxycholecalciferol) enhances paclitaxel antitumor activity in vitro and in vivo and accelerates paclitaxel-induced apoptosis. Clin Cancer Res. 2001; 7:1043–1051. [PubMed: 11309356]

Jayaweera AR, Edwards N, Glasheen WP, Villanueva FS, Abbott RD, Kaul S. In-vivo myocardial kinetics of air-filled albumin microbubbles during myocardial contrast echocardiography: comparison with radiolabeled red blood cells. Circ Res. 1994; 74:1157–1165. [PubMed: 8187282]

Kaul S. Myocardial contrast echocardiography. A 25 year perspective. Circulation. 2008; 118:291–308. [PubMed: 18625905]

Li YS, Davidson E, Reid CN, McHale AP. Optimising ultrasound-mediated gene transfer (sonoporation) in vitro and prolonged expression of a transgene in vivo: Potential applications for gene therapy of cancer. Cancer Lett. 2009; 273:62–69. [PubMed: 18829156]

Maeda H, Tominaga K, Iwanaga K, Nagao F, Habu M, Tsujisawa T, Seta Y, Toyoshima K, Fukuda J, Nishihara T. Targeted drug delivery system for oral cancer therapy using sonoporation. J Oral Pathol Med. 2009; 38:572–579. [PubMed: 19549112]

Meijering BD, Juffermans LJ, van Wamel A, Henning RH, Zuhorn IS, Emmer M, Versteilen AM, Paulus WJ, van Gilst WH, Kooiman K, de Jong N, Musters RJ, Deelman LE, Kamp O. Ultrasound and microbubble-targeted delivery of macromolecules is regulated by induction of endocytosis and pore formation. Circ Res. 2009; 104:679–687. [PubMed: 19168443]

Nayak S, Herzog RW. Progress and prospects: immune responses to viral vectors. Gene Ther. 2010; 17:295–304. [PubMed: 19907498]

Nie F, Xu HX, Lu MD, Wang Y, Tang Q. Anti-angiogenic gene therapy for hepatocellular carcinoma mediated by microbubble-enhanced ultrasound exposure: An in vivo experimental study. J Drug Target. 2008; 16:389–395. [PubMed: 18569283]

Parryl JJ, Sharma V, Andrews R, Moros EG, Piwnica-Worms D, Rogers BE. PET imaging of heat-inducible suicide gene expression in mice bearing head and neck squamous cell carcinoma xenografts. Cancer Gene Ther. 2009; 16:161–170. [PubMed: 18758434]

Price RJ, Skyba DM, Kaul S, Skalak TC. Delivery of colloidal particles and red blood cells to tissue through microvessel ruptures created by targeted microbubble destruction with ultrasound. Circulation. 1998; 98:1264–1267. [PubMed: 9751673]

Rainov NG. A phase III clinical evaluation of herpes simplex virus type 1 thymidine kinase and ganciclovir gene therapy as an adjuvant to surgical resection and radiation in adults with previously untreated glioblastoma multiforme. Hum Gene Ther. 2000; 11:2389–2401. [PubMed: 11096443]

Reinhold HS, Visser JW. In vivo fluorescence of endothelial cell nuclei stained with the bis-benzamide H33342. Int J Microcirc Clin Exp. 1983; 2:143–146. [PubMed: 6678844]

Shand N, Weber F, Mariani L, Bernstein M, Gianella-Borradori A, Long Z, Sorensen AG, Barbier N. A phase 1–2 clinical trial of gene therapy for recurrent glioblastoma multiforme by tumor transduction with the herpes simplex thymidine kinase gene followed by ganciclovir. Hum Gene Ther. 1999; 10:2325–2335. [PubMed: 10515452]

Thomas SM, Grandis JR. The current state of head and neck cancer gene therapy. Hum Gene Ther. 2009; 8:2110–2120.

van Wamel A, Bouakaz A, Versluis M, de Jong N. Micromanipulation of endothelial cells: Ultrasound-microbubble-cell interaction. Ultrasound Med Biol. 2004; 30:1255–1258. [PubMed: 15550330]

Villanueva FS, Wagner WR. Ultrasound molecular imaging of cardiovascular disease. Nature Clin Prac Cardiovasc Med. 2008; 5:26–32.

Villanueva FS. Ultrasound mediated destruction of DNA-loaded microbubbles for enhancement of cell-based therapies: New promise amidst a confluence of uncertainties? J Am Coll Cardiol Imaging. 2009; 2:880–882.

Weller G, Villanueva FS, Klibanov AL, Wagner WR. Modulating targeted adhesion of an ultrasound contrast agent to dysfunctional endothelium. Ann Biomed Eng. 2002; 30:1012–1019. [PubMed: 12449762]

Weller GE, Wong MK, Modzelewski RA, Lu E, Klibanov AL, Wagner WR, Villanueva FS. Ultrasonic imaging of tumor angiogenesis using contrast microbubbles targeted via the tumor-binding peptide RRL. Cancer Res. 2005; 65:533–539. [PubMed: 15695396]

Zhao S, Ferrara KW, Dayton PA. Asymmetric oscillation of adherent targeted ultrasound contrast agents. Appl Phys Lett. 2005; 87:134103–134106.

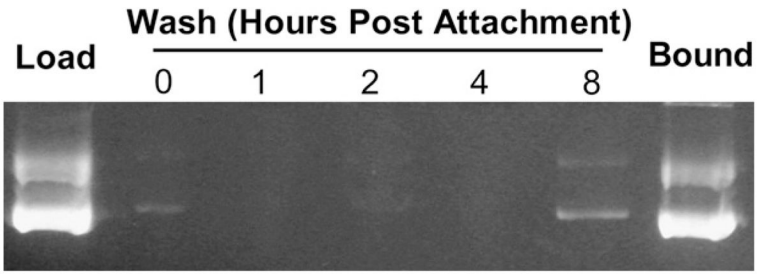

Fig. 1.

Agarose gel electrophoresis demonstrating efficient DNA binding to microbubble and lack of plasmid release over time. Microbubbles loaded with DNA were washed immediately to remove unbound DNA (0 hours), and washed again at 1, 2, 4 and 8 h post attachment (the washes are in lanes 2 to 6). Washed microbubbles were destroyed and bound DNA was recovered after all washes were complete at 8 h (“Bound,” lane 7). Lane 1 contains 500 ng plasmid as a loading control.

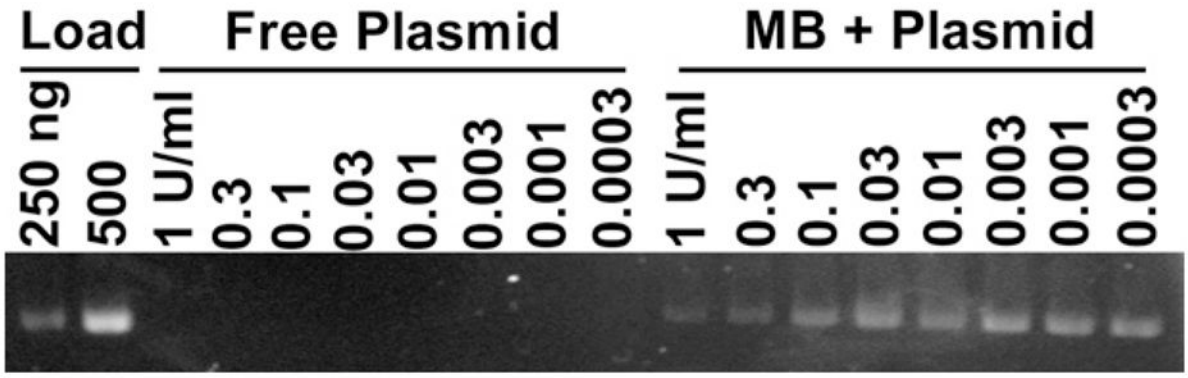

Fig. 2.

Agarose gel electrophoresis demonstrating the resistance of DNA bound to microbubbles against digestion by DNAses. Microbubbles loaded with DNA were washed three times to remove unbound DNA and subjected to a range of DNAseI concentrations from 0.0003 U/mL to 1 U/mL (lanes 11 to 18). As a control, free plasmid DNA was also challenged with DNAseI at these same concentrations (lanes 3 to 10). Lanes 1 and 2 contain 250 ng and 500 ng plasmid as loading controls.

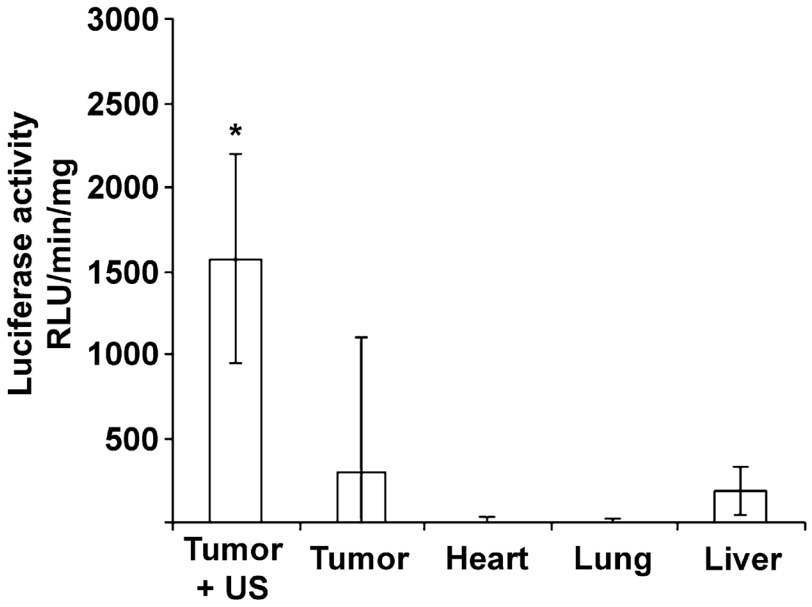

Fig. 3.

Luciferase activity in murine squamous cell carcinoma and control tissues 3 d after intravenous delivery of pCMV-luc bound to microbubbles. Mice from the Tumor + US sample were treated with ultrasound directed to the tumor. Nontargeted heart, lung and liver samples were obtained from the ultrasound-treated mice, and control tumor samples were obtained from a separate group receiving plasmid-loaded microbubbles but no ultrasound (*$p < 0.02$).

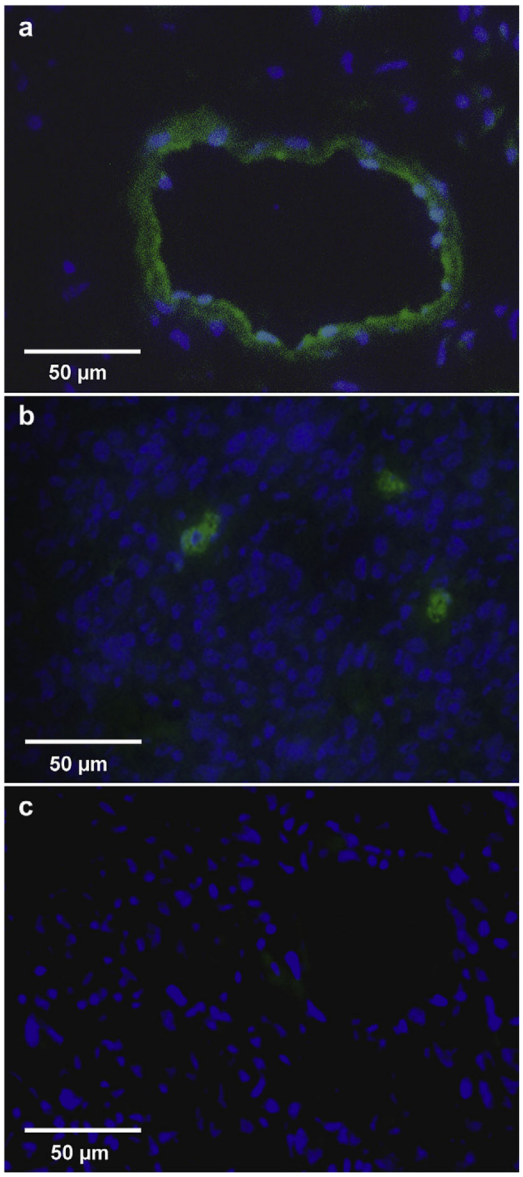

Fig. 4.

Immunofluorescent staining of GFP in murine tumors 3 d after intravenous delivery of pEGFP-C1 bound to microbubbles and treatment with ultrasound (a, b) or no ultrasound (c). GFP-positive staining was seen both in hollow structures (a) as well as individual tumor cells (b) in UTMD-treated tumors.

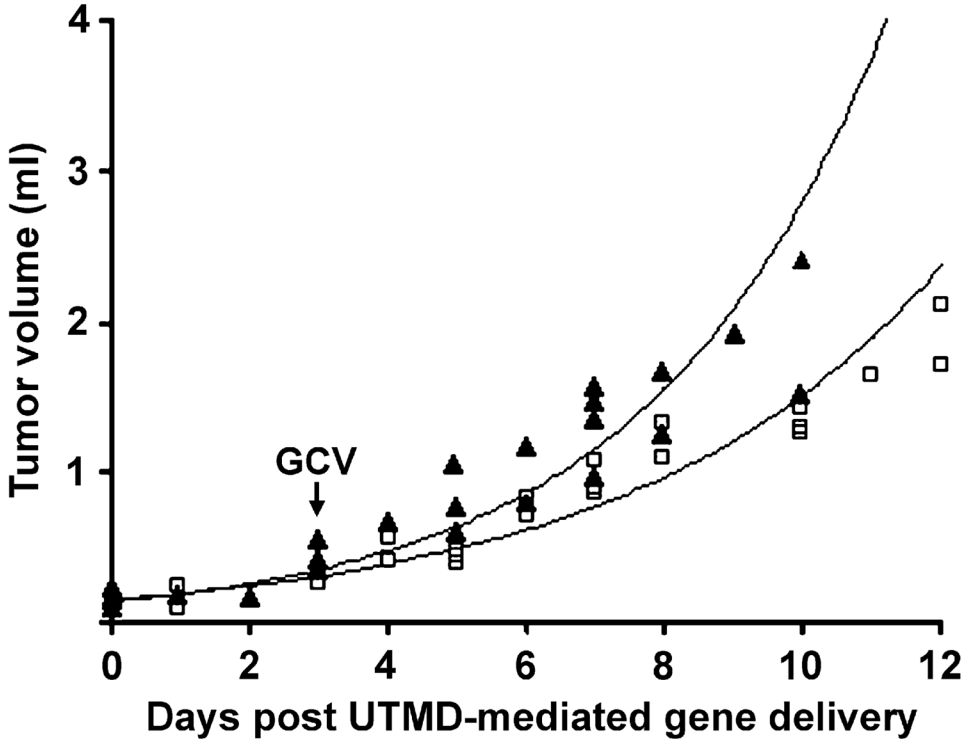

Fig. 5.

Growth of murine tumors after intravenous injection of either pCMV-TK (□) or pEGFP-C1 (▲)-loaded microbubbles and treated with ultrasound. Daily GCV injections began on day 3. Best-fit lines were calculated from all data points in each group assuming an exponential growth curve (TK $R^2 = 0.94$; GFP $R^2 = 0.91$).

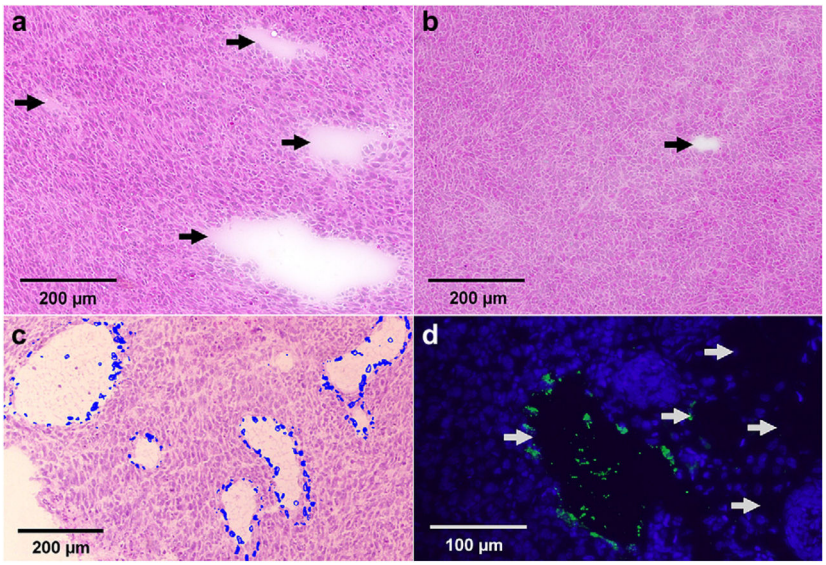

Fig. 6.

Postmortem histology of tumors after intravenous delivery of either pCMV-TK (a, c, d) or pEGFP-C1 (b)-loaded microbubbles and treatment with ultrasound and GCV. (a, b) Acellular zones (*arrows*) visible under H&E stain. (c) Merged image of two sister slides, one stained by Heoscht 33342 (*blue overlay*) and one stained by H&E. (d) Variable vWF staining in acellular zones (*arrows*).

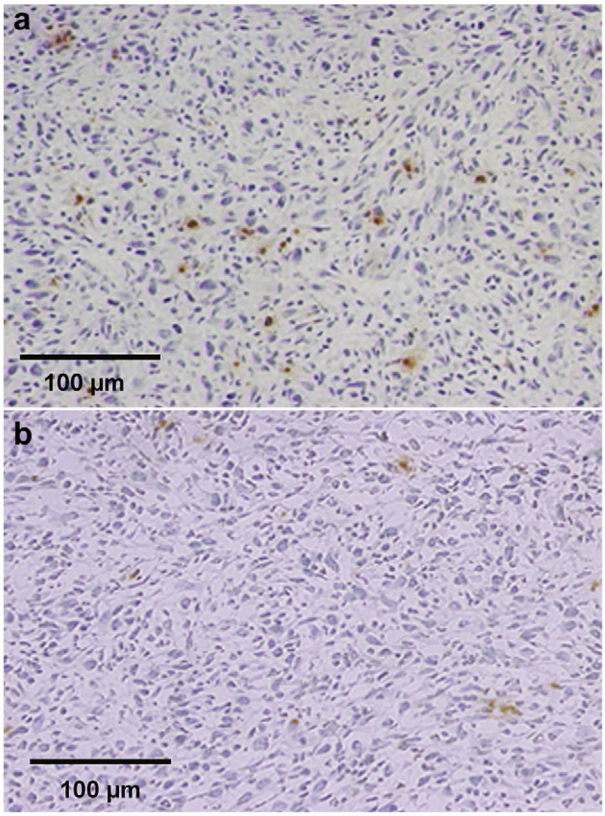

Fig. 7.

Postmortem TUNEL assays from murine tumors after intravenous injection of either pCMV-TK (a) or pEGFP-C1 (b)-loaded microbubbles and treatment with ultrasound and GCV.